Comparative Design Study of a Diesel Exhaust Gas Heat Exchanger for Truck Applications with Conventional and State of the Art Heat Transfer Enhancements

S. Mavridou[(1)], G.C. Mavropoulos[(2)], D. Bouris[(1)*], D.T. Hountalas[(2)], G. Bergeles[(2)]

[(1)] Department of Mechanical Engineering, University of Western Macedonia, Bakola&Sialvera, 50100, Kozani, Greece.

[(2)] School of Mechanical Engineering, National Technical University of Athens, Heroon Polytechniou, 15710, Athens, Greece.

Abstract

The exhaust gas of heavy duty diesel engines can provide an important heat source that may be used in a number of ways to provide additional power and improve overall engine efficiency. The sizing of a heat exchanger that can manage the heat load and still be of reasonable size and weight without excessive pressure drop is of significant importance especially for truck applications. This is the subject of the present work. To approach the problem, a total of five different configurations are investigated and a comparison of conventional and state of the art heat transfer enhancement technologies is included. Two groups of configurations are examined: a) a classical shell and tube heat exchanger using staggered cross flow tube bundles with smooth circular tubes, finned tubes and tubes with dimpled surfaces, and b) a cross flow plate heat exchanger, initially with finned surfaces on the exhaust gas side and then with 10 ppi and 40 ppi metal foam material substituting for the fins. Calculations were performed, using established heat exchanger design methodologies and recently published data from the literature to size the aforementioned configurations. The solutions provided reduce the overall heat exchanger size, with the plate and fin type consisting of plain fins presenting the minimum pressure drop (up to 98% reduction compared to the other configurations), and the 40 ppi metal foam being the most compact in terms of size and weight. Durability of the solutions is another issue which will be examined in a future investigation. However, coupling of the exhaust heat exchanger after a particulate trap appears to be the most promising solution to avoid clogging from soot accumulation.

Keywords: Heat exchanger, Exhaust gas, Diesel engine, Truck, Heat transfer

[*] Corresponding Author: Tel.: +30 24610 56675, *Email address*: dmpouris@uowm.gr

NOMENCLATURE

A, area [m^2]

b, height [m]

C_p, specific heat [J/kgK]

D_{HEX}, W_{HEX}, L_{HEX}, streamwise, spanwise (cylinder axis or plate width) directions and height of heat exchanger [m]

d, diameter [m]

F, correction factor

f, friction factor

h, heat transfer coefficient [W/m^2K]

l , length [m]

$\dot{m}$, fluid flow rate [kg/s]

N, number (of tubes, baffles etc)

Nu Nusselt number

n, efficiency

P, pitch [m]

Pr, Prandtl number

$\dot{Q}$, volumetric flow rate [m^3/s]

Re, Reynolds number

R_f, fouling resistance [m^2K/W]

R_{th}, thermal resistance [m^2K/W]

St, Stanton number

T, temperature [^oC]

t, thickness [m]

U, specific volume [m^3/kg]

u, velocity [m/s]

V, volume [m^3]

$\dot{W}$, pumping power [W]

Greek symbols

α, cubic unit cell size [m]

β, total heat transfer area/volume between plates [m^2/m^3]

ΔP, pressure drop [Pa]

η, increment coefficient for dimpled tubes

λ, thermal conductivity [W/mK]

μ_s, air viscosity at the tube wall temperature [kg/ms]

ν, kinematic viscosity [m^2/s]

ρ, density [kg/m^3]

φ, viscosity correction factor

Subscripts

b, baffles

c, cold-fluid side of heat exchanger

cb, convective boiling

col, columns

cross, cross flow

cyl, cylinder of the metal foam cubic unit cell

d, dimple

dt, dimpled tube

eq, equivalent

f, fin

fr, frontal

free, free flow

ft, finned tube

HEX, heat exchanger

h, hot-fluid side of heat exchanger

heat, heat transfer area

hyd, hydraulic

i, inner

MF, metal foam

m, mean conditions

min, minimum

nb, nucleate boiling

o, outer

p, plates

pf, plain fins

p-f, plate and fin

row, rows

s, shell side

st, smooth tube

s-t, shell and tube

TP, two phase

t, tube side

tb, tube bank

tot, total

w, wall

1, inlet

2, outlet

Acronyms

bsfc brake specific fuel consumption= (fuel consumption rate)/(power), [$^{gr}/_{W}^{s}$]

1. Introduction

Despite recent improvements of diesel engine efficiency, a considerable amount of energy is still expelled to the ambient from the exhaust gas. This, depending on engine operating conditions, is in the order of 30-40% of fuel consumption. For this reason, considerable improvement of diesel engine bsfc can be achieved through the utilization of exhaust gas energy and a number of technical solutions and possibilities have been proposed and are currently under investigation by research institutes and engine manufacturers. In the case of heavy duty diesel engines suitable for truck applications, one of the most promising technical solutions for exhaust gas waste heat utilization appears to be the use of a "Bottoming Rankine Cycle".

A systematic approach towards using an installation based on the Rankine Cycle in truck applications dates back to the early 70's where a research program funded by the US Department of Energy (DOE) was conducted by Mack Trucks and Thermo Electron Corporation [1], [2], [3]. Under this program, an Organic Rankine Cycle System (ORCS) was installed on a Mack Truck diesel engine and the lab test results revealed an improvement of bsfc of 10-12%, which was verified by highway tests. During the following years similar research programs were performed by other research institutes and vehicle manufacturers. Recently, the solution of Rankine Cycle systems has increased its potential competitiveness in the market even more [4], [5]. This is a result of technical advancements in a series of critical components for the operation of such an installation (heat exchanger, condenser, expander) but also stems from the highly increased fuel prices. Nowadays, the installation of a Rankine Cycle is not only considered as a feasible solution for efficiency improvement in heavy duty diesel engines for trucks [6], [7] but also for smaller applications such as passenger cars [8].

With the exception of turbo-compounding, most existing solutions for the partial recovery of exhaust heat utilize a heat exchanger to extract energy from the exhaust gas. A heat exchanger used in such an application has to be able to provide an adequate surface area in order to handle the thermal duty while meeting the specifications of a small-size and lightweight arrangement. Still, the incurred pressure drop has to be of reasonable magnitude to avoid excessive pumping power losses that will have a negative impact on net engine efficiency.

Heat transfer enhancement can be achieved either by increasing the volume specific heat transfer area of the heat exchanger or by increasing the heat transfer coefficient of the exhaust gas flow. Several approaches to the problem can be found in the literature. The surface of a plain circular tube can be increased using fins [9], [10] and since it is well known that the heat transfer coefficient on the gas side is much lower than on the liquid side, the finned heat transfer surfaces are usually used on the gas side to increase the heat transfer area. Several types of fins are used to enhance heat exchange, such as plain circular fins, slotted fins, punched and bent triangular projections, segmented fins, etc. One of the earliest and yet highly effective techniques is the use of tube surface roughness. Much of the early work focused on 'naturally' occurring roughness in commercial tubes. However, as pointed out by Bergles [11], because such natural roughness is not well defined, artificial or structured roughness is now commonly employed in most applications. Structured roughness can be integral to the surface, or the protuberances can be introduced in the form of wire-coil-type inserts. Sherrow et al. [12] presented experimental results regarding the effects of adding either deep or shallow spherical-indentation dimples to the exterior surfaces of tubes in a four row staggered tube bundle under cross-flow. They found that the deep dimples produced significant heat transfer augmentations (compared to tubes with smooth exterior surfaces) for tubes located in the tube row which was farthest upstream. The shallow dimples produced significant heat transfer augmentations on the tubes which were located in the first, third and fourth rows of the tube bundle. Bouris et al. [13] proposed the usage of tubes of non-circular cross section. They compared, numerically and experimentally, a typical industrial in-line tube bundle arrangement with an elliptic and drop-shaped arrangement in terms of thermal and hydraulic characteristics as well as particle deposition rates. The research showed that the drop-shaped tube bundle design that they proposed not only attained higher heat transfer levels but also resulted in much lower deposition rate and lower pressure drop. Daloglu and Unal [14] proposed the upstream positioning of an obstacle of a circular or square cross-section with the same or different diameter as the tube in order to alter the heat transfer from the tube. They concluded that at high Reynolds numbers the heat transfer from the test cylinder behind an obstacle becomes considerably higher than that of a single cylinder. Boomsma et al. [15] used open-cell metal foams from aluminum alloy which were compressed and

fashioned into compact heat exchangers and then placed into a forced convection arrangement using water as a coolant. These were compared to commercially available heat exchangers on the basis of required pumping power versus thermal resistance. The compressed aluminum foams performed well, not only in heat transfer enhancement, but also in terms of efficiency over the commercially available heat exchangers operating under nearly identical conditions. The metal foam heat exchangers decreased the thermal resistance by nearly half when compared to conventional heat exchangers designed for the same application.

The purpose of the present work is a comparative approach to the exhaust gas heat exchanger design problem. Although the ultimate application is that the heat exchanger be a part of a Rankine Cycle, the present study is not concerned with details of the cycle and focuses on the usage of different heat exchanger configurations and different types of heat transfer surfaces. Implementing well established methodologies as well as recently published technological advances, a numerical algorithm is developed to perform preliminary sizing calculations and compare five different heat exchanger arrangements. Comparisons are performed in terms of the provided heat transfer area, the volume and weight of the arrangement as well as the induced pressure drop and the energy required during operation of the system. The arrangements studied are a shell and tube type heat exchanger consisting of either smooth, dimpled or finned circular tubes, and a plate and fin type, where plain fins or metal foam are used as a means of heat transfer area extension. The final results are given in form of tables and diagrams. For the comparison of the various heat exchanger solutions as far as weight and pressure drop are concerned, a qualitative approach is adopted due to the parametric nature of the present investigation.

2. Problem Definition and Data

The heat exchanger design problem requires input data regarding diesel engine exhaust gas conditions and Rankine Cycle working medium conditions, which is taken from other parallel studies [16] - [19]. The engine considered in the present work is a six-cylinder heavy-duty turbocharged truck engine. It has a bore of 125 mm, a stroke of 140 mm and a compression ratio of 16.5:1. The engine is equipped with a common-rail

fuel injection system allowing the variation of both injection pressure and injection advance. In the present investigation, injection pressure was maintained at the standard level and the maximum power of the diesel engine is 362 kW at 1700rpm. A schematic layout of the proposed Rankine Cycle installation with water as working media is provided in Figure 1. The heat exchanger is employed after the engine turbocharger to produce steam, which is expanded in the next stage to produce energy in an electric generator. One important characteristic of the present installation is that it utilizes heat from the EGR (Exhaust Gas Recirculation) stream which is otherwise wasted during cooling. This is accomplished by leading the steam produced in the heat exchanger through the EGR cooler, which is used essentially for superheating.

The theoretical aspects of the present installation have been investigated using detailed simulation models both for diesel engine [16], [17] and Rankine Cycle operation [18]. Due to the complexity of the application, the full scope cannot be covered here but a brief description follows and available details can be found in the above mentioned references. One of the most important findings of the simulation was that when introducing the Rankine Cycle with water as working medium, the potential efficiency gain was estimated in the range of 6-10% (for 100% engine load), depending on the environmental conditions. To accomplish this task with water as working medium, the results of the previous investigation revealed that due to the low mass flow rate values, in combination with the high pressure operation of the cycle, a reciprocating expander is the only possible solution for delivering the additional power. Due to the introduction of the Rankine cycle, an additional radiator is necessary to reject the excess heat to the environment. Results from the detailed simulation revealed that it is beneficial for the second radiator to be installed behind the diesel engine main radiator (just in front of the engine) and not vice-versa. The aforementioned utilization of EGR heat is beneficial towards the reduction of the excess heat rejection to the ambience. This minimizes the negative impact on overall efficiency because the additional power required to drive the cooling fan is kept to a minimum. For the feeder pump a positive displacement type was found to be the most feasible solution. Concerning the working media, which for the present application is water, it has been revealed from detailed investigations using organic media for the Rankine Cycle (i.e. methanol, R245ca, C6F6 etc) that it does not have a significant effect on the overall heat exchanger sizing and

efficiency. The previous devices, together with other supplementary components, were calculated and sized in detail for the specific diesel engine and Rankine cycle installation. From these results, the ones corresponding to the calculation and sizing of the heat exchanger (as one of the most critical components) will be presented in the present study.

To account for the potential benefit from the use of an exhaust gas recuperation system, a wide set of engine operating conditions was considered in the investigation, which almost entirely covered the engine operating map. This set of operating conditions is presented in Table 1. From the data presented in this table, it is observed that the highest rate of heat load on the heat exchanger corresponds to the engine operating point of 100% load and 1300 rpm engine speed. For this reason the heat exchanger geometry calculations were performed with data and parameter values corresponding to this engine operating condition. The maximum flow velocities and temperature differences are taken from typical truck engine operating conditions [19] and the final set of data is given in Table 2. The values of parameters which appear in Table 2 are considered to remain constant for all configurations during calculations.

Assuming that the recovered heat will be delivered to the closed Rankine cycle, the heat exchanger is separated into three different functional areas: a) preheater, b) evaporator, c) superheater. Calculations are carried out separately for each heat exchanger component and the final results are derived from the sum of all three values. Regarding weight calculation, unless otherwise stated, the material for all parts of the shell&tube heat exchangers is steel (ρ_{steel}=8000 kg/m^3), while the shell thickness for all configurations is 2 mm.

3. Numerical Procedure

A numerical algorithm is developed to perform the sizing calculations:

- The Bell – Delaware method is implemented for sizing shell&tube heat exchangers [9],
- Schmidt's method is used to calculate tube fin efficiency [9],
- Dimpled tube air-side heat transfer coefficient has been taken from [12],

- Plate&fin sizing is based on Kays and London [20],
- A metal foam filled plate heat exchanger was sized based on data adapted from Lu et al. [21], Klein et al. [22] and ERG corporation [23],
- The evaporation heat transfer coefficient in tubes of the shell&tube exchangers is calculated according to Shah's method [24],
- The Logarithmic Mean Temperature Difference method LMTD is used to calculate heat output [9],
- The pumping power required to operate each system of heat exchangers is calculated as the product of pressure drop and volume flow rate.

Using methods defined in the literature [20] - [25], the overall pressure drop and weight are estimated. For economy of space and since most of the design methodologies are well established, only application-specific modifications will be presented in detail, providing the reader with appropriate and adequate references for the rest. As already mentioned, due to the comparative nature of the approach, results are provided on a relative basis for both parameters.

3.1. Shell and Tube Heat Exchanger

3.1.1. Plain Circular Tubes

The first case examined is that of a shell and tube heat exchanger consisting of smooth circular tubes. Figure 2 shows the heat exchanger under consideration where, for clarity, only a few tubes have been drawn in their (30^o) triangular arrangement in the shell with P_{row} being the distance between the tube rows and P_{col} the distance between the tube columns. The working media considered herein is water or steam which flows inside the tubes and exhaust gas flows around them. However, even though the use of this system is problematic when using a turbine expander, due to the low volumetric flow rate, the results are valid even if an organic medium is used. This is verified from simple calculations already conducted revealing that heat exchanger area does not differ considerably when organic medium is used instead of water.

For the sizing process, a number of parameters like the shell diameter, the tube diameter, the tube distance etc. have to be defined. The problem is open-ended i.e. any

combination of shell and tube diameter and length that provides the required heat output is a solution. Here, a maximum outer shell diameter of 0.49 m has been considered a reasonable limit for the present application. Also, a staggered arrangement tube bundle with tube diameter d_t=16 mm has been maintained. Based on this data, an iterative process between the Bell-Delaware method and Eq. (1) - (3) is adopted until convergence for the heat transfer coefficient and the heat transfer area is achieved. An initial geometry is chosen for the exchanger (height, depth, tube length, tube pitch, number of tubes, etc.) in order to calculate the heat transfer coefficient of the preheater and superheater from Eq. (3) (the evaporator is subject to a different methodology, described below). This value of (h) is then set in Eq. (1) and if the required heat output is not met, modifications of geometry are made and the process is repeated until the values of Table 3 are attained. Eq. (1), (2) and (3) define the heat output (Q), the logarithmic mean temperature difference (LMTD) and the total heat transfer coefficient ($h_{tot,st}$) respectively:

$$Q = h_{tot,st} \cdot A_{heat,tot} \cdot F \cdot LMTD \tag{1}$$

$$LMTD = \frac{(T_{h,2} - T_{c,1}) - (T_{h,1} - T_{c,2})}{\ln \frac{T_{h,2} - T_{c,1}}{T_{h,1} - T_{c,2}}} \tag{2}$$

$$h_{tot,st} = \frac{1}{\frac{1}{h_s} + R_{f,s} + \frac{t_w}{\lambda_w} \cdot \frac{2 \cdot d_{t,o}}{d_{t,o} + d_{t,i}} + (R_{f,t} + \frac{1}{h_t}) \cdot \frac{d_{t,o}}{d_{t,i}}} \tag{3}$$

The correction factor (F) appearing in Eq. (1) is available in chart form in [26] while Eq. (3) is taken from Kuppan [9]. The shell side heat transfer coefficient (h_s) takes into account the leakage effects, according to the Bell-Delaware method [9]. For applications such as the present, it is extremely difficult to find accurate data for the fouling resistances (R_f) appearing in Eq. (3), but indicative values have been assumed in order to partially account for the fouling effects [24]: $R_{f,s}=1.761 \cdot 10^{-3}$ m^2K/W for all areas in contact with the exhaust gas, $R_{f,t}=1.76 \cdot 10^{-4}$ m^2K/W for the preheater tube side

and $8.8 \cdot 10^{-5}$ m^2K/W for the evaporator and superheater tube side. It should be kept in mind however that no effort has been made to differentiate fouling behaviour among the heat exchanger configurations being investigated and so the above mentioned values will be used throughout. Finally, it may be noted that these values may be an optimistic assumption but they should be judged taking into account that the heat exchanger is placed after a soot trap (Figure 1), whose efficiencies are commonly over 90% and even 99% in some cases, without significant dependence on particle size ([27], [28])

In most cases, it is the gas side heat transfer coefficient that mainly affects the total value in Eq. (3), even though the present application imposes laminar flow conditions inside the tubes. In the present configuration as well as those following, heat transfer from both hot and cold streams is included in the calculations. For laminar single phase flow ($Re \cong 360\text{-}1000$), the tube side heat transfer coefficient, h_t, is given by the correlation ([10]):

$$h_t = \frac{1.86(Re_t \cdot Pr_t \cdot d_{t,i} / l_t)^{1/3} \cdot \varphi^{0.14} \cdot \lambda_t}{d_{t,i}}, \qquad \varphi = (\mu_t/\mu_m)^{0,14} \tag{4}$$

In the evaporator, two-phase flow in the tubes must be taken into account in the overall heat transfer coefficient calculation. Thus, the widely used method of Shah [24] is adopted, in which convective and nucleate boiling contributions are calculated separately and then combined:

$$h_{TP} = h_{cb} + h_{nb} \tag{5}$$

Analytical description of Shah's method can be found in Kakac and Liu ([24]). Calculations are performed for at least 10 mixture qualities between 0 -1 (pure liquid – pure vapor) and the final h_{TP} results from averaging the heat transfer coefficients for each mixture quality.

Pressure drop of shell&tube heat exchangers consisting of plain circular tubes is given by Kakac and Liu ([24]):

$$\Delta P_{s\text{-}t,st} = \frac{f \cdot \left(\dot{m}_s / A_{cross} \right) \cdot (N_b + 1) \cdot d_s}{2\rho_s \cdot d_{eq} \cdot \varphi}, \quad f = \exp(0.576\text{-}0.19 \ln Re_s), \quad \varphi = (\mu_s/\mu_m)^{0.14} \tag{6}$$

where (f) is the friction coefficient for the shell and (φ) is the viscosity correction factor. The friction coefficient accounts for the entrance and exit losses, while the Reynolds number on the shell side, Re_s, is provided by

$$Re_s = \frac{\left(\dot{m}_s / A_{cross} \right) \cdot d_{eq}}{\mu_s} \tag{7}$$

where the thermo physical properties are evaluated at the average fluid temperature in the shell. The equivalent diameter on the shell side (d_{eq}) depends on the pitch layout. For a triangular pitch-layout (as used here),

$$d_{eq} = \frac{4\left(\frac{(P_{col})^2 \sqrt{3}}{4} - \frac{\pi d_{t,o}{}^2}{8} \right)}{\frac{\pi d_{t,o}}{2}} + \frac{4\left(\pi/4\right)\left(d_s{}^2 - d_{tb,o} \right)}{\frac{\pi d_{t,o}}{2} N_t} \tag{8}$$

A common means to measure the heat convection effectiveness is the thermal resistance (R_{th}). Lower thermal resistance facilitates the heat flow through the heat exchanger. The common definition for (R_{th}) in a heat convection arrangement is:

$$R_{th} = \frac{T_w - T_{h,1}}{\dot{m}_h \cdot C_{p,h} \cdot (T_{h,2} - T_{h,1})} \tag{9}$$

The numerator is the tube wall-gas temperature difference and the denominator is the heat load. Taking into account that these remain constant in the present study, all types of heat exchangers considered will have the same thermal resistance. Comparison will thus focus on size, weight and the energy required to operate the system, i.e. pumping power. The required pumping power ($\dot{W}$) is calculated according to

$$\dot{W} = \Delta P \cdot \dot{Q}_h \,, \quad \dot{Q}_h = \frac{\dot{m}_h}{\rho_h} \tag{10}$$

with ($\dot{Q}_h$) indicating the volumetric flow rate of the hot-side fluid (exhaust gas) passing through the heat exchanger.

Finally, the total volume of the shell&tube heat exchanger consisting of smooth circular tubes is

$$V_{s\text{-}t,st} = \frac{\pi \cdot D_{HEX}{}^2 \cdot l_t}{4} \tag{11}$$

3.1.2. Finned Circular Tubes

The case of circular tubes with external, circumferential fins is also examined. Based on the configurations provided by [20], the following fin dimensions are chosen: fin height (b_f=6.044·10^{-3} m), fin thickness (t_f=2.5395·10^{-4} m) and fin spacing (P_f=2.9178 ·10^{-3} m). Figure 3 shows a tube bundle of finned circular tubes and the cross section of a finned tube. For comparison purposes, shell and tube diameter are considered the same as in the previous case. To calculate the heat transfer coefficient of the finned tubes, Schmidt's method [9] is adopted, according to which the total heat transfer coefficient from the finned tubes is:

$$h_{tot,ft} = \frac{1}{\frac{1}{h_s \cdot n_s} + \frac{R_{f,s}}{n_s} + \frac{t_w}{\lambda_w} \cdot \frac{2 \cdot A_{ft}}{\pi \cdot \left(d_{t,o} + d_{t,i}\right)} + \left(R_{f,t} + \frac{1}{h_t}\right) \frac{A_{ft}}{\pi \cdot d_{t,i}}} \tag{12}$$

The shell side heat transfer coefficient (h_s) is calculated from Kays and London [20], in the same way as in the case of the plain tubes and assumes that all effects included in the Bell Delaware method (leakage ratios etc) affect the shell side heat transfer coefficient (h_s), but not the surface efficiency (n_s). Eq. (4) is applied for the tube side

heat transfer coefficient in single phase flow with $Re \le 2300$ while for $2300 \le Re \le 10000$ ([10])

$$h_t = \frac{0.116(Re_t^{2/3} - 125) \cdot Pr^{1/3} \varphi^{0.14} \cdot \left[1 + \left(\frac{d_{t,i}}{l_t}\right)^{2/3}\right] \lambda_t}{d_{t,i}} \tag{13}$$

For the evaporator, Shah's method (Eq. 5) is applied. The surface efficiency on the shell side of the heat exchanger (n_s) is given by

$$n_s = 1 - \frac{A_{f/l_t}}{A_{ft/l_t}} \cdot (1 - n_f) \tag{14}$$

where the fin surface per unit of tube length ($A_{f/lt}$) and the finned tube surface per unit of tube length ($A_{ft/lt}$) are:

$$A_{f/l_t} = (2\pi \cdot \left(\left(\frac{d_{ft,o}}{2}\right)^2 - \left(\frac{d_{ft,i}}{2}\right)^2\right) + 2\pi \cdot \frac{d_{ft,o}}{2} \cdot t_f) \cdot \frac{l_t}{P_f} \tag{15}$$

$$A_{ft/l_t} = 2\pi \frac{d_{t,o}}{2} l_t + 2 \cdot \left[\pi \cdot (\frac{d_{t,o}}{2} + b_f)^2 - \pi \left(\frac{d_{t,o}}{2}\right)^2\right] \cdot \frac{l_t}{P_f}$$

Also, the fin efficiency is

$$n_f = \frac{\tanh(m \cdot l^*)}{(m \cdot l^*)} \tag{16}$$

with

$$l^* = \left(\frac{d_{ft,o}}{2} - \frac{d_{ft,i}}{2}\right) \cdot \left[1 + \frac{t_f}{2 \cdot \left(\frac{d_{ft,o}}{2} - \frac{d_{ft,i}}{2}\right)}\right] \cdot \left[1 + 0,35 \cdot \ln \frac{d_{ft,o}}{d_{ft,i}}\right], \qquad m = \sqrt{\frac{2 \cdot h_s}{\lambda_f \cdot t_f}} \tag{17}$$

Pressure drop calculations are carried out for circular finned tubes type "CF-8.7-5/8J", for the preheater, evaporator and superheater, based on [9]:

$$\Delta P_{s-t,ft} = 4f \cdot \frac{d_s}{d_{hyd}} \frac{\left(\dot{m}_s / A_{free,min} \right)^2}{2\rho_s} \tag{18}$$

The friction factor (f) is taken from diagrams given by Kays and London [20] and includes entrance and exit effects. The required pumping power is calculated from Eq. (10) and the total volume of the arrangement is given from Eq. (11).

3.1.3. Dimpled Circular Tubes

Rough tubes have also been examined as a means of heat transfer augmentation while, for comparison purposes, shell and tube diameter are considered the same as in the previous cases. Roughness is accomplished by locating either shallow or deep dimples on the exterior tube surface, as shown in Figure 4. Sherrow et al. [12] also suggest a relation between Reynolds number on the shell side and Nu/Nu_o – where Nu_o is the shell side Nusselt number referring to smooth tubes. Considering that $Nu = h \cdot d_t / \lambda_s$ then for constant tube diameter (d_t) and air thermal conductivity (λ_s), one can calculate the heat transfer ratio $\left(h_{s,dt} / h_{s,st} \right)$ from the Nusselt number ratio $\left(Nu_{s,dt} / Nu_{s,st} \right)$. Preserving Reynolds number similarity, the total heat transfer coefficient for the dimpled tubes can be derived, including the dimple effects on the shell-side

$$h_{s-t,dt} = \frac{1}{\frac{1}{(h_{s,st})\eta} + \frac{R_{f,s}}{\eta} + \frac{t_w}{\lambda_w} \cdot \frac{2 \cdot d_{t,o}}{d_{t,o} + d_{t,i}} + \left(R_{f,t} + \frac{1}{h_t} \right) \frac{d_{t,o}}{d_{t,i}}} \tag{19}$$

where the increment coefficient, η, takes the values shown in Table 4. Eq. (4) is applied for the tube side heat transfer coefficient in single phase flow while for the evaporator, Shah's method (Eq. 5) is applied. Exact relations could not be found for the pressure drop in case of the dimpled tubes but according to Chudnovsky and Kozlov [25] tubes with exterior surface dimples cause shell side pressure drop that varies between -20% to +10% from the corresponding pressure drop that plain circular tubes induce. This range is used for comparison with the other configurations and is an additional reason for providing pressure drop results as normalized values. Finally, the pumping power is given by Eq. (10) while the total volume arises again from Eq. (11).

3.2 Plate and Fin Heat Exchanger

3.2.1. Plain Fins

The second group of heat exchangers examined in the present work is the plate and fin type. A plate&fin heat exchanger is shown in Figure 5. As in the case of the shell&tube type, virtually any combination of height, width and depth is possible. Here, a constant cross section of 0.63x0.63 m^2 has been chosen for the exhaust side. For the present calculations triangular fins are used, having the characteristics (for both the hot and cold side) shown in Table 5, as described by Kays and London [20]. These fins have been used in order to suit the geometry and the arrangement first chosen.

The total heat transfer coefficient $h_{p\text{-}f,pf}$ of this type of heat exchanger is calculated as [20]:

$$\frac{1}{h_{p-f,pf}} = \frac{1}{n_h \cdot h_h} + \frac{R_{f,h}}{n_h} + \frac{1}{\frac{A_c}{A_h} \cdot n_c \cdot h_c} + \frac{R_{f,c}}{n_c} \cdot \frac{A_h}{A_c} + \frac{t_p}{\lambda_p} \cdot \frac{A_h}{A_p} \tag{20}$$

The heat transfer coefficient on each side in Eq. (20) is given by,

$$h = St \cdot \frac{\dot{m}}{A_{free}} \cdot C_p \tag{21}$$

where St, $\dot{m}$, A_{free} and C_p are calculated accordingly for the hot and cold fluid. The Stanton number, St, is taken from diagrams corresponding to the basic characteristics of the surface [20] and provided in the form of $St \cdot Pr^{2/3}$, as a function of Reynolds number ($Re = \frac{d_{hyd} \cdot (\dot{m}/A_{free})}{\mu}$). For the evaporator, and since correlations for two-phase heat transfer coefficients for water are not readily available, both Shah's method (Eq. 5) and several of the correlations examined in [29] were applied, showing a maximum difference of 20%. For simplicity, and acknowledging the limitations concerning plate instead of tubular geometry, Shah's method was applied for the calculation of the water side boiling heat transfer coefficient. Also,

$$A_{free} = \sigma \cdot A_{core} \quad , \sigma = a \cdot \frac{d_{hyd}}{4} \quad , \quad a = \frac{P_p \cdot \beta}{P_{p,h} + P_{p,c} + 2t_p} \tag{22}$$

where σ is the ratio of the free-flow area to the frontal area. The total heat transfer area on each side is

$$A_{heat} = a \cdot V_{HEX} \tag{23}$$

and the total volume of the heat exchanger is $V_{HEX} = (W \cdot D \cdot l)_{HEX}$. The surface efficiency (n) is calculated for both the cold and hot sides:

$$n = 1 - \frac{A_f}{A_{heat,tot}} \cdot (1 - n_f) \tag{24}$$

The fin efficiency (n_f) for cold and hot sides is given by Eq. (16), where (l^*) is replaced by $P_p/2$. Pressure drop of plate&fin heat exchangers is given by Kays and London [20]:

$$\Delta P_{p-f,pf} = \frac{\left(\dot{m}_h / A_{cross}\right)}{2} U_{h,1} \left[\left(1 + \sigma^2\right) \left(\frac{U_{h,2}}{U_{h,1}} - 1 \right) + f \frac{A_h}{A_{h,free}} \frac{U_m}{U_{h,1}} \right] \tag{25}$$

In Eq. (25), entrance and exit loss effects are accounted for in the friction factor (f) which is provided by [20] in terms of Reynolds number. Moreover, (U_m) is calculated from

$$U_m = (U_{h,1} + U_{h,2})/2 \quad (26)$$

Mass calculations are performed using steel as the fin material. Eq. (10) gives the pumping power, as in the previous cases.

3.2.2. Metal Foam

The use of open-celled metal foams is a new trend in applications where packaging is important i.e. truck applications (small dimensions and low weight). These advantages of metal foam are examined herein. The multi-layer compact plate-and-fin type heat exchanger of Figure 6 is considered, where exhaust gas and cold water flow alternately in cross-flow. For every other passage of thickness dW, where exhaust gas flows between two thin plates, an open-celled nickel foam core replaces the fins that would appear in a standard plate-and-fin heat exchanger (grey area). Figure 7a shows one of the passages filled with metal foam.

For the heat exchanger design, it is highly desirable to have data over a wide range of operating conditions. This is not readily available for metal foam and so the present model has adopted the equation form of Lu et al. [21], who considered that the open-celled foam is made up of uniform distributed, equal-sized cubic cells. The actual cell shape is more complex [30] but the cubic unit cell has been chosen for its simplicity and the analytical expression to limit the complexity of calculating forced convective flow across an open-celled foam. Such an assumption may lead to an overestimation of the actual level of heat transfer but nevertheless, according to Lu et al. [21], the trends of heat transfer predicted by the model are expected to be valid for a wide range of open-cell foams and correction for this overestimation will be applied subsequently. The simple cubic unit cell shown in Figure 7b is assumed to consist of three mutually perpendicular equivalent cylinders each having diameter d and length α. The cylinders

making up the cell edges are assumed to be each parallel to the x, y or z coordinate. Lu et al. [21] mention a 4-fold overestimation for the total heat transfer coefficient, and so their analytical solution has been modified accordingly:

$$h_{MF} = \frac{\sqrt{3\pi}}{4} \cdot \left(\frac{\lambda_{MF}}{\alpha} \right) \left(0.3 \mathrm{Pr}^{1/3} \frac{\lambda_h}{\lambda_{MF}} \right)^{1/2} \left(\frac{u_h \alpha}{v_h} \right)^{0.3} \frac{\left(\rho_{MF} / \rho_{solid} \right)^{1/2}}{\left(\frac{\alpha}{d_{cyl}} - 1 \right)^{0.3}} \tag{27}$$

Parameter (d_{cyl}) is given by [21] as a function of cell size (α) and relative foam density, defined as the ratio of foam density and the density of the solid. It is noted that Eq. (27) is expressed per unit interface (plate) area and so, the total heat transfer coefficient $h_{p\text{-}f,MF}$ of this type of heat exchanger is:

$$\frac{1}{h_{p-f,MF}} = \frac{1}{h_{MF}} + R_{f,h} \cdot \frac{A_{interface}}{A_{MF}} + \frac{1}{\frac{A_c}{A_{interface}} \cdot n_c \cdot h_c} + \frac{R_{f,c}}{n_c} \cdot \frac{A_{interface}}{A_c} + \frac{t_p}{\lambda_p} \cdot \frac{A_{interface}}{A_p} \tag{28}$$

As far as the fouling resistance on the hot side of this heat exchanger is concerned, it has to be pointed out that calculations are made using the values already mentioned, as there are no available published data for metal foams.

Calculations are carried out using two types of metal foam: a) 10 ppi, with relative foam density 0.09 and cell size α = 2 mm, which give cylinder diameter d_{cyl} = 0.39 mm and b) 40 ppi, with the same relative foam density and cell size α = 0.5 mm, which lead to d_{cyl} = 0.09 mm. The heat output is calculated from Eq. (1), where the heat transfer area used refers to the plate/foam-metal interface area ($A_{interface}$):

$$A_{interface} = D_{HEX} \cdot L_{HEX} \cdot (N_p - 1) \tag{29}$$

The exhaust gas velocity is calculated from

$$\dot{m}_h = \rho_h \cdot u_h \cdot A_{cross} \tag{30}$$

where

$$A_{cross} = \left[L \cdot dW - \frac{L \cdot dW \cdot d_{cyl}}{\alpha} - \frac{dW^2 \cdot d_{cyl}}{\alpha} + \frac{L \cdot dW \cdot d_{cyl}^{\ 2}}{\alpha^2} \right] \cdot \left(\frac{N_p - 1}{2} \right) \quad (31)$$

Eq. (27) [21] is in general agreement with the data calculated by computational fluid dynamics simulation in [30] for the 40 ppi foam but it underestimates the heat transfer coefficient by ~ 25% if the exhaust gas side is filled with a 10 ppi foam. Therefore some "fine tuning" of Eq. (27) is performed for the 10 ppi foam by introducing a multiplier of 1.25. The two phase heat transfer coefficient was dealt with in the same way as in the plate&fin heat exchanger.

For the pressure drop calculation of plate heat exchangers using metal foam to fill the space between plates on the exhaust gas side, Eq. (25) is used [20]. The friction factor (f) in the aforementioned equation is calculated from pressure drop data of ERG Corporation [23] for 10 ppi and 40 ppi metal foam. In order to calculate the free flow area ($A_{h,free}$) on the exhaust gas side, values of the ratio $A_{free}/A_{frontal}$ calculated by Kopanidis et al. [30] were used and found very close to the value of the porosity of the material.

As far as the mass calculation is concerned, the metal foam material was nickel, with a density of 8906 kg/m^3. Commonly used aluminum metal foam was not considered as an option due to the high exhaust gas temperatures utilized in the current application. The shell and plate thickness, as for all previous configurations, is 2 mm. The required pumping power is given from Eq. (10) and the total volume of the plate&fin type heat exchanger with metal foam is $V_{HEX} = (D \cdot W \cdot l)_{HEX}$.

4. Results

The results of all calculations conducted are presented in Table 6 (a,b) and Figure 8-Figure 11. In Figure 8 the total volume, relative mass and relative pressure drop for each of the heat exchangers are shown with respect to the shell and tube heat exchanger consisting of smooth circular tubes (considered as the standard solution with mass m_o

and pressure drop ΔP_o). The heat exchangers are ranked on the x-axis from left to right, according to their mass. One can easily discern that the most common shell and tube type configuration, consisting of smooth circular tubes, is the heaviest solution while it results in the greatest pressure drop (except for a potentially higher pressure drop caused by the dimpled tubes). When roughness is introduced by means of dimples on the exterior tube surface, the overall mass and weight as well as the pressure drop of the configuration are reduced, but further reduction of the mass and pressure drop can be achieved by introducing fins on the tubes' external surface. The finned tubes reduce the overall weight and pressure drop by ~51% and ~45% respectively, but the total volume is slightly increased by 8% since a larger spacing is required between the tubes, to accommodate for the fins.

If the standard plate and fin type heat exchanger is compared with the shell and tube heat exchanger with finned tubes, there is a significant (~66.5%) advantage in terms of volume, but the mass is increased by 20.6%. Moreover, there is a remarkable reduction in pressure drop. This may be attributed to the fact that, for the plate type heat exchangers with fins or metal foam, an effort was made to keep the frontal area constant at ~0.6x0.6 m and vary only the depth, leading to very shallow heat exchanger configurations between 2.5 and 10.3 cm (Table 6). When the fins are replaced by 10 ppi metal foam on the exhaust gas side, there is a 30.4% reduction in mass while the total volume increases by ~6.7%. Pressure drop increases significantly, but this is still the next best configuration. Replacing the 10 ppi foam with a 40 ppi foam, leads to a 96% increase in the pressure drop but the mass and volume are further reduced (35% and 42% respectively). In fact, the 40 ppi foam plate heat exchanger is the most compact arrangement having less than 30% of the volume of the initial shell and tube configuration with plain tubes.

With regard to pressure drop it should be mentioned that the equations that have been employed address tube bundle and plate-fin pressure drop, including bundle or finned channel entrance and exit effects but no other pressure drops that may arise from header losses, leakages, flow passage through bends etc.

The different heat exchanger types in the present work are being compared for the same heat output, which permits direct conclusions to be drawn concerning their compactness. This is extremely important when the heat exchanger is to be installed on

a mobile application such as a truck. As a consequence, both its geometric dimensions and weight are equally important because they strongly affect the net truck freight load and its fuel consumption. However, it should be mentioned that the final fuel consumption also depends strongly on the pressure drop induced by the heat exchanger and thus this should be carefully considered. Figure 9 and Figure 10 show the relative pumping power as a function of relative mass and the heat output per unit volume, respectively. In Figure 9 (where W_o refers to the pumping power needed in the shell and tube heat exchanger with smooth circular tubes) the best design in terms of pumping power is the one that lies closer to the origin of the axes. In this case, it is the 40 ppi plate and fin (foam) heat exchanger that consumes 68% less power to drive the exhaust gas past the device, compared to the shell and tube heat exchanger with smooth tubes, and weighs 73% less. This configuration also provides the highest heat output per unit volume at four fold the value of the shell and tube heat exchanger with plain tubes (Figure 10) and, with a total volume of ~45 lt, it is a potential under-the-hood design. The standard plate and fin design still operates with the least pumping power but its overall volume is almost 1.7 times that of the 40 ppi foam (44.8 lt). The main advantage of the 40 ppi metal foam stems from the increased heat transfer area achieved by the foam (165.08 m^2, as shown in Table 6b). There is a large area to volume ratio and therefore reduced size, accompanied by a 42%-68% reduction in the pressure drop and pumping power as well, compared to the shell and tube configurations. For comparison, the heat transfer coefficient and the friction factor are plotted in Figure 11 for each of the heat exchanger configurations studied. It is noted that the heat transfer coefficients are expressed per unit total heat transfer area (and not interface area as presented in Table 6), in order to provide a common basis for comparison. It is interesting to note that in terms of heat transfer and pressure drop coefficients, the metal foam heat exchangers seem to be at a disadvantage but in fact, due to their high area/volume ratio, they result in the most compact and lightweight solutions. Some scattering of the heat transfer coefficient values in the shell&tube designs, notably low values for the superheater, is due to the low heat transfer values resulting from the change to gas phase (steam) on the tube side. This is not pronounced for the finned tubes where the tube side area is a small percentage of the total (finned) heat transfer area and therefore the reduction has a negligible effect on the overall heat transfer coefficient. The tube side

effect is also less apparent in the plate&fin designs for another reason: the crossflow design permits a reduction in frontal area on the steam side (see D dimension in Figure 5 and Table 6b) leading to higher Reynolds numbers and a consequential increase in heat transfer, which partially compensates for the reduction due to the phase change. The assumed constant tube diameter in the shell&tube designs does not allow for such compensation.

The above mentioned values must be considered in a comparative sense and within the scope of the uncertainty in the data and the available calculation methodologies. Indicatively, Bell and Mueller [31] state that although the Bell-Delaware method is considered to be the best in the open literature, it has been shown to predict shell-side heat transfer coefficients within 50% to 100% of measured values. On the other hand, in the present work, sensitivity of the calculated volume of the shell and tube heat exchangers to values chosen for necessary data such as the baffle hole clearances was found negligible as long as TEMA recommendations are adhered to [9]. For finned tubes, Schmidt's method gives a fin efficiency value within 1% of the exact value [9] while for dimpled tubes, the uncertainty in the Nusselt number ratio is ±12.6% [12]. For the metal foam data values, cross-checking with published experimental values gave uncertainties in heat transfer coefficients below 30%.

5. Conclusions

The present work deals with the sizing of a diesel engine exhaust gas heat exchanger for truck applications. For this reason the exchanger must not only be able to extract considerable amounts of heat from the engine exhaust but must also have acceptable dimensions and weight. For this reason it is necessary to minimize the volume and weight of the arrangement, while at the same time maintaining the heat transfer from the gas side at a maximum.

To approach the problem, a comparative design study with conventional and state of the art heat transfer enhancements was conducted. Two different heat exchanger configurations with different types of heat transfer surfaces have been examined regarding their weight, volume, induced pressure drop and their effect on the vehicle (freight weight etc.). The shell and tube configuration was examined first consisting

initially of smooth, and then finned and dimpled circular tubes in order to increase the heat transfer area. The plate and fin was the second configuration studied, where plain fins or metal foam (10 ppi and 40 ppi) were examined as a means of heat transfer.

To account for the most severe condition calculations were based on the consideration that the heat exchanger operates under conditions corresponding to the maximum exhaust thermal load (100% load, 1300 rpm). The heat exchanger was separated into three different functional areas: a) preheater, b) evaporator, c) superheater. Calculations were carried out for each one of the areas separately and the results came from the addition of the three values.

A numerical algorithm based on established heat exchanger design methodologies and recently published data from the literature was developed. Aiming at achieving a pre-defined value for the heat output produced by each part of the heat exchangers and following an iterative process, the heat transfer coefficient and the heat transfer area were calculated along with an analytical specification of the parameters necessary to define the heat exchanger arrangement. Results indicate that the lowest pressure drop is achieved by the standard plate and fin arrangement but if size and weight are also taken into account then substituting the fins with metal foam leads to a 38% reduction in volume and a twofold reduction in weight for the 40 ppi foam. Unfortunately, this results in an increase of pumping power (pressure drop) compared to the finned plates but still lower than all the shell and tube designs. Therefore it appears that there is a possibility to develop a heat exchanger that can satisfy both energy and volume constraints being suitable for truck applications. The standard shell&tube solutions examined herein can provide a basis for the development of more advanced heat exchangers suitable for truck applications.

Finally, the fact that future diesel engines are to be equipped with particulate traps makes the use of a heat exchanger more attractive because indications exist that heat exchanger fouling may not be so severe.

ACKNOWLEDGEMENTS

The authors would like to acknowledge funding by the EU under the FP6 research program Green Heavy Duty Engine", "TIP4-CT-2005-516195".

References

[1] Parimal P.S. and Doyle E.F., Compounding the truck diesel engine with an organic Rankine cycle system, SAE Paper No. 760343 (1976).

[2] Dibella F.A., Di Nanno L.R. and Koplow M.D., Laboratory and on-highway testing of diesel organic Rankine compound long-haul vehicle engine, SAE Paper No. 830122 (1983).

[3] Doyle E., Di Nanno L. and Kramer S., Installation of a diesel-organic Rankine compound engine in a class 8 truck for a single-vehicle test, SAE Paper No. 790646 (1979).

[4] Kadota M. and Yamamoto K., Advanced Transient Simulation on Hybrid Vehicle Using Rankine Cycle System, SAE Paper No. 2008-01-0310 (2008).

[5] Hounsham S., Stobart R., Cooke A. and Childs P., Energy Recovery Systems for Engines, SAE Paper No. 2008-01-0309 (2008).

[6] Nelson C., Exhaust Energy Recovery, 2008 Diesel Engine-Efficiency and Emissions Research (DEER) Conference, Dearborn, Michigan, August 4-7, 2008.

[7] Kruiswyk R.W., An Engine System Approach to Exhaust Waste Heat Recovery, 2008 Diesel Engine-Efficiency and Emissions Research (DEER) Conference, Dearborn, Michigan, August 4-7, 2008.

[8] Ringler J., Seifert M., Guyotot V. and Huebner W., Rankine Cycle for Waste Heat recovery of IC Engines, SAE Paper No. 2009-01-0174 (2009).

[9] Kuppan T., Heat Exchanger Design Handbook, Marcel Dekker Inc. (2000).

[10] Bejan A. and Kraus A., Heat Transfer Handbook, Wiley & Sons (2003).

[11] Bergles, A. E., Techniques to Enhance Heat Transfer (1998) in Handbook of Heat Transfer, 3rd ed., (Rohsenow W. M., Hartnett, J. P., and Cho, Y. I., eds.), McGraw-Hill, New York, Chap. 11.

[12] Sherrow L., Ligrani P., Chudnovsky Y. and Kozlov A., "Effects of Exterior Surface Dimples on Heat Transfer and Friction Factors for a Cross-Flow Heat Exchanger", Journal of Enhanced Heat Transfer, Vol. 13 (2006) pp. 1-15.

[13] Bouris D., Konstantinidis E., Balabani S., Castiglia D. and Bergeles G., Design and Evaluation of a Novel, Intensified Heat Exchanger for Particle Deposition Rate Reduction, International Journal of Heat And Mass Transfer, Vol. 48 (2005) pp. 3817-3832.

[14] Daloglu A. and Unal A., Heat Transfer from a Cylinder in the Wake Flow, Int. Comm. Heat Mass Transfer, Vol. 27, No. 4 (2000) pp. 569-580.

[15] Boomsma, K., Poulikakos, D., Zwick, F., Metal foams as high performance heat exchangers, Mechanics of Materials, Vol. 35 (2003) pp. 1161-1176.

[16] Hountalas, D.T., Mavropoulos, G.C., Zannis, T.C. and Schwarz, V. (2005a) Possibilities to Achieve Future Emission Limits for HD DI Diesel Engines using Internal Measures, SAE Paper No. 2005-01-0377.

[17] Hountalas, D.T., Mavropoulos, G.C. and Binder, K.B, Effect of exhaust gas recirculation (EGR) temperature for various EGR rates on heavy duty DI diesel engine performance and emissions, *Energy*, Vol. 33, 2 (2008), pp. 272-283.

[18] Hountalas, D.T., Katsanos, C.O., Kouremenos, D.A. and Rogdakis, E.D., Study of available exhaust gas heat recovery technologies for HD diesel engine applications, *Intern. J. of Alternative Propulsion*, Vol. 1, No.2/3 (2007), pp. 228–249.

[19] Hountalas D.T. and Katsanos C., Integrated Project: Green Heavy Duty Engine. National Technical University of Athens, School of Mechanical Engineering, Thermal Engineering Section. TIP4-CT-2005-516195 (2006).

[20] Kays W.M. and London A.L., Compact Heat Exchangers, Krieger Publishing Company (1984).

[21] Lu T.J., Stone H.A. and Ashby M.F., "Heat Transfer in Open-cell Metal Foams", Acta mater, Vol. 46, No. 10 (1998) pp. 3619-3635.

[22] Klein J.F., Arcas N., Gilchrist G.W., Shields W.L., Yurman R. and Whiteside J.B., "Thermal Management of Airborne Early Warning and Electronic Warfare Systems Using Foam Metal Fins", Technology Review Journal, Spring/Summer 2005 (2005).

[23] ERG, Materials and Aerospace Corporation. http://www.ergaerospace.com

[24] Kakac S. and Liu H. Heat Exchangers, Selection, Rating and Thermal Design. CRC Press (1998).

[25] Chudnovsky Y. and Kozlov A., Development and field trial of dimpled-tube technology for Chemical industry process heaters. Final report, U.S. DOE Award DE-FC07-01ID14089 (2006).

[26] Kakac S. Boilers, Evaporators and Condensers. Wiley, New York (1991).

[27] Cauda E, Fino D, Saracco G, Specchia V, Secondary nanoparticle emissions during diesel particulate trap regeneration, Topics in Catalysis, 42–43, pp. 253-257, (2007)

[28] Biamino S., Fino P., Fino D., Russo N. and Badini C., Catalyzed traps for diesel soot abatement: In situ processing and deposition of perovskite catalyst, Applied Catalysis B: Environmental, 61, 3-4, pp. 297-305, (2005)

[29] Garcia-Cascales J.R., Vera-Garcia F., Corberan-Salvador J.M., Gonzalvez-Macia J. Assessment of boiling and condensation heat transfer correlations in the modelling of plate heat exchangers, Int. J. Refrigeration, 30, pp. 1029-1041 (2007)

[30] Kopanidis A., Theodorakakos A., Gavaises E., Bouris D., Numerical Simulation of Fluid Flow and Heat Transfer with Direct Modelling of Microscale Geometry, 5th European Thermal-Sciences Conference, The Netherlands (2008).

[31] Bell K.J. and Mueller A.C., Wolverine Engineering Data Book II, Wolverine Tube, Inc. (2001).

Figure Captions

Table Captions

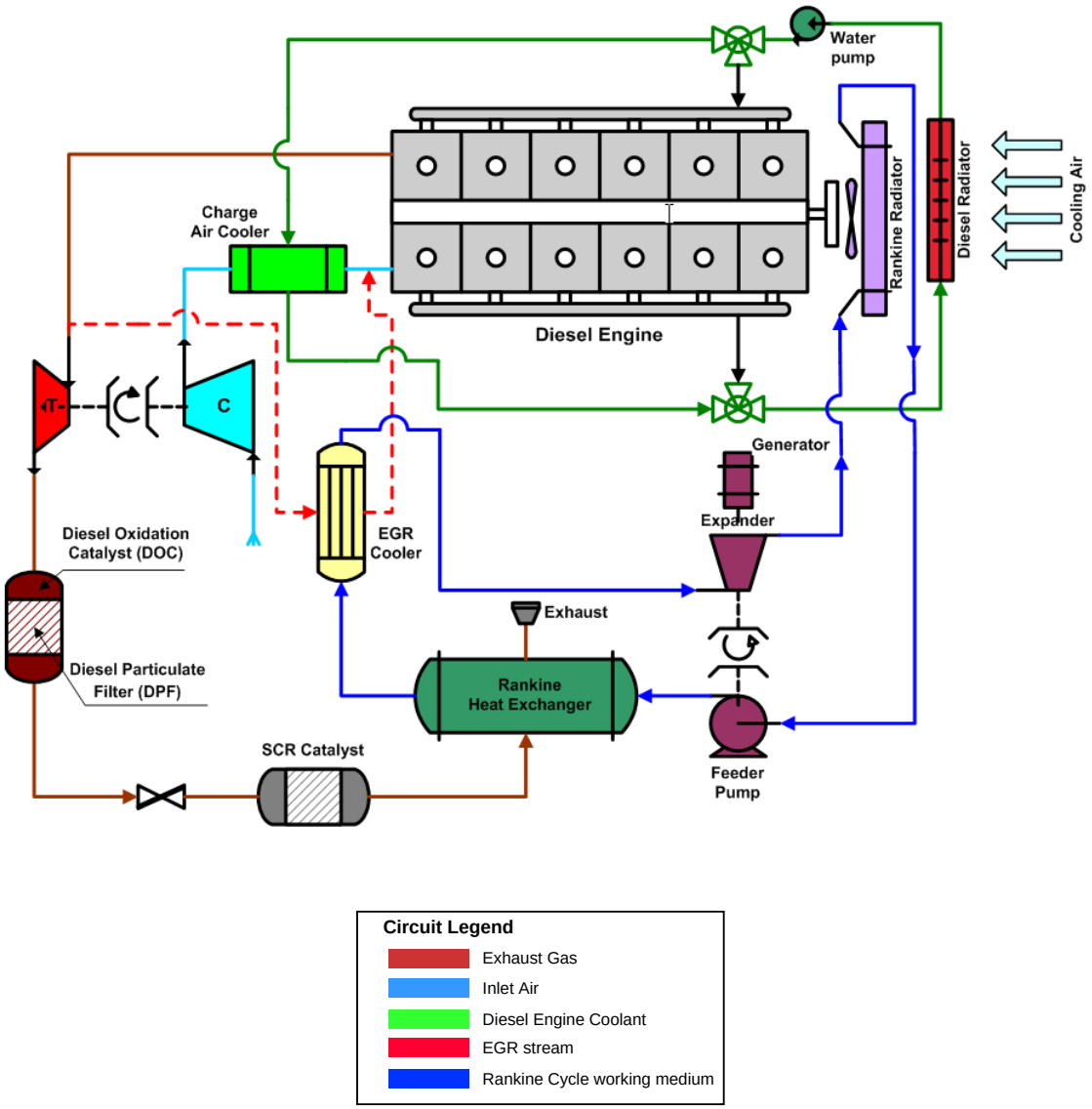

Figure 1. Schematic view of the proposed layout of Rankine cycle installation. Working media: steam.

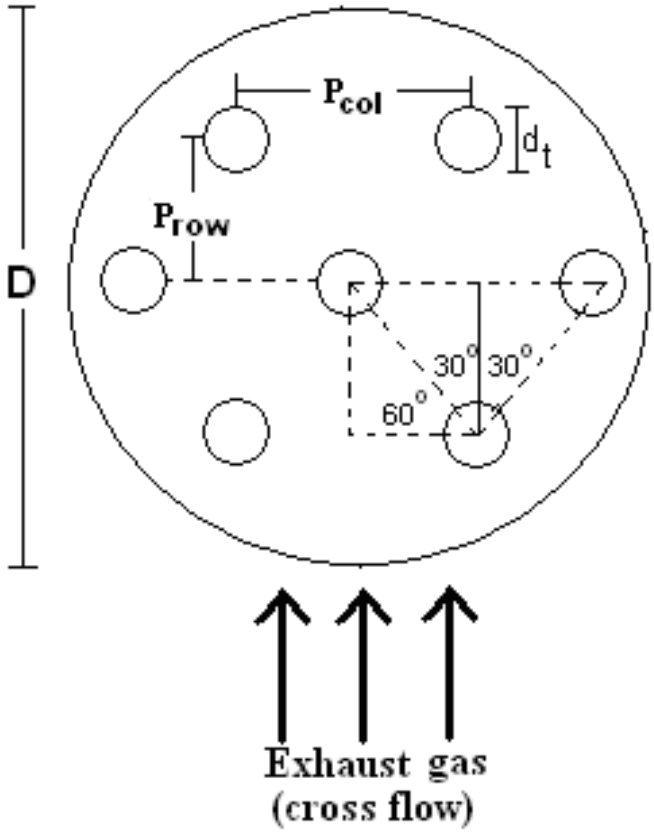

Figure 2. Heat exchanger with smooth circular tubes.

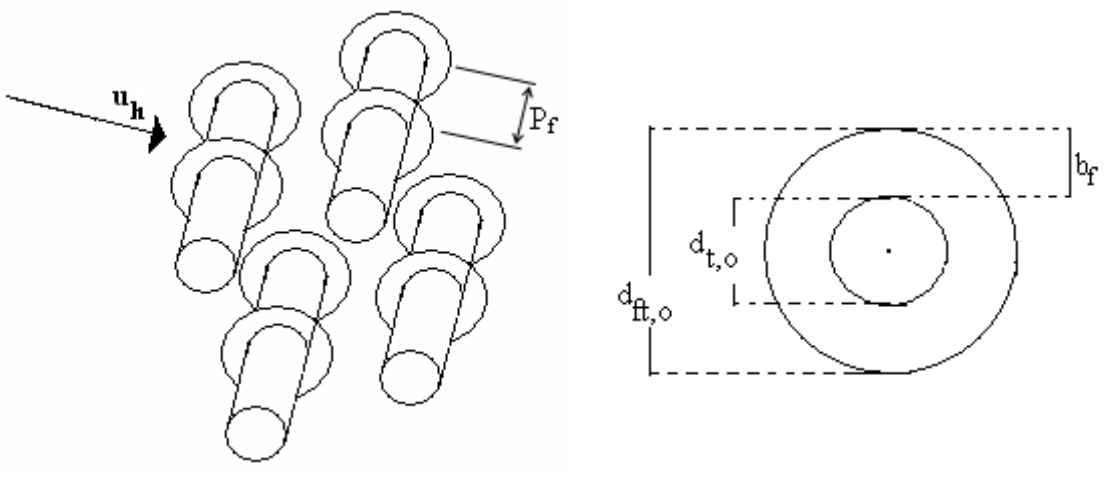

(a) (b)

Figure 3. a) Tube bundles of finned circular tubes. (b) Schematic diagram of a finned tube.

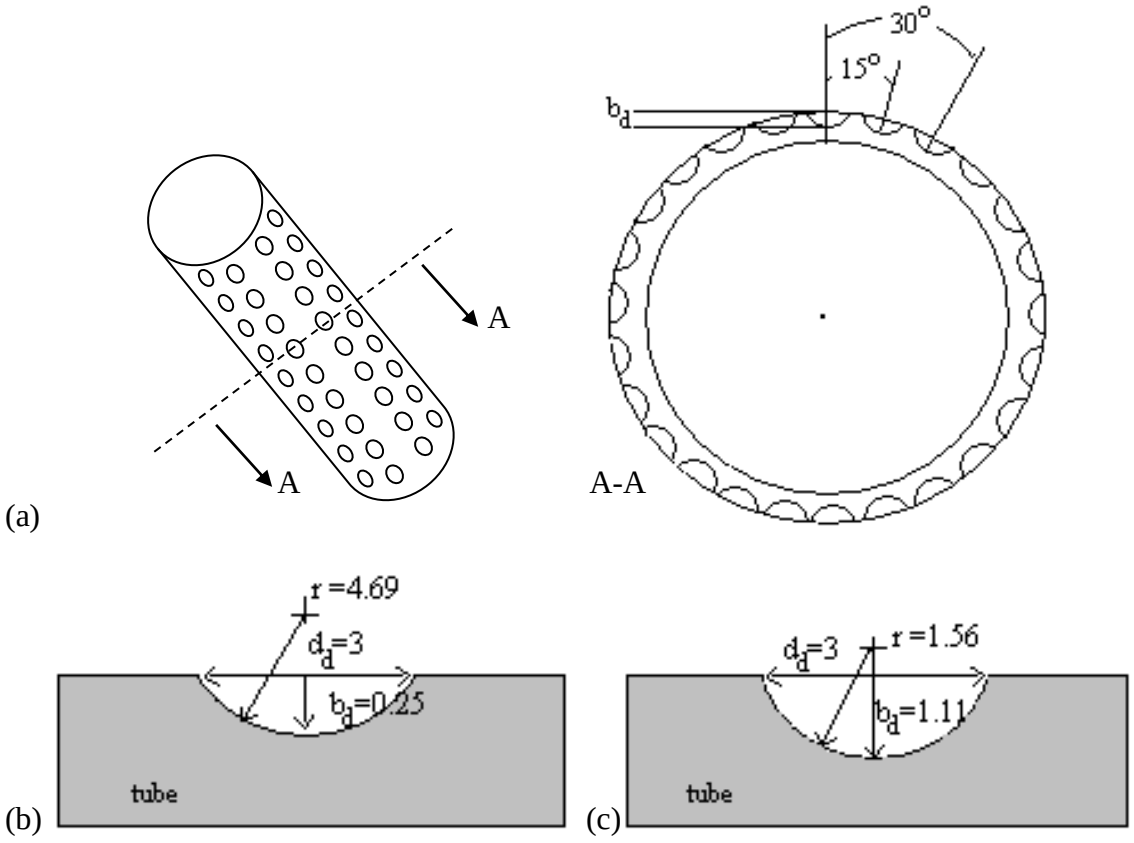

Figure 4. Schematic diagrams showing (a) cross section of a dimpled tube. (b) details of a dimple geometry for shallow dimples. (c) details of a dimple geometry for deep dimples (dimensions are in millimeters).

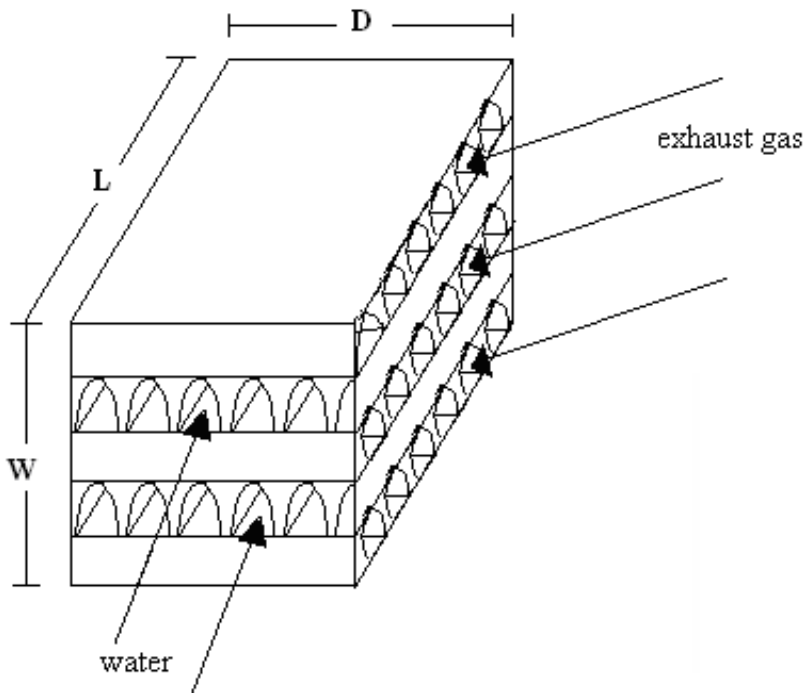

Figure 5. Plate-and-fin heat exchanger.

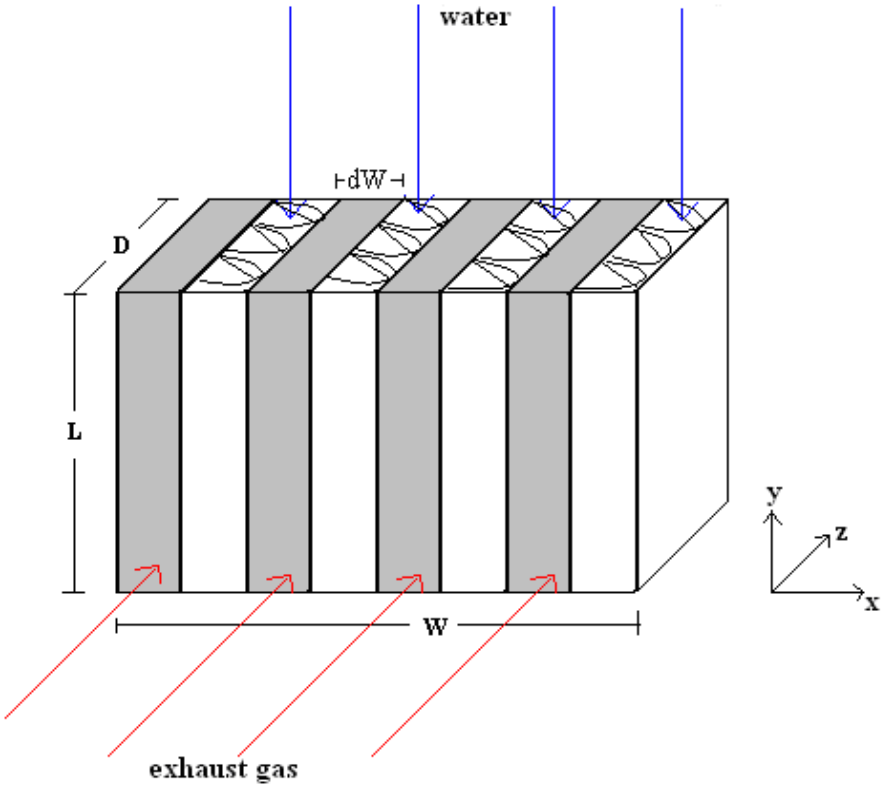

Figure 6. Plate and fin heat exchanger with metal foam.

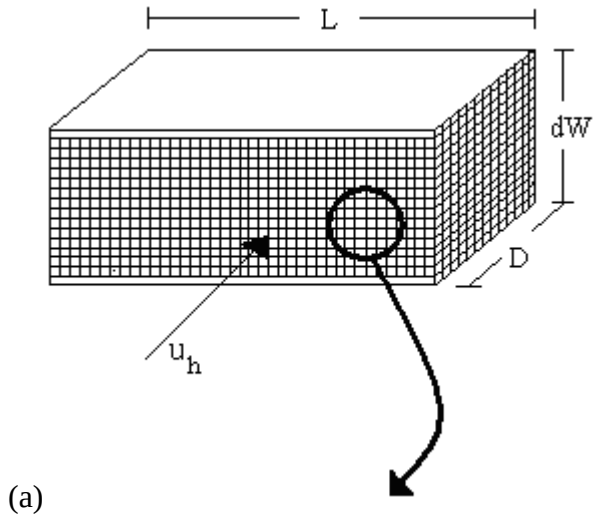

(a)

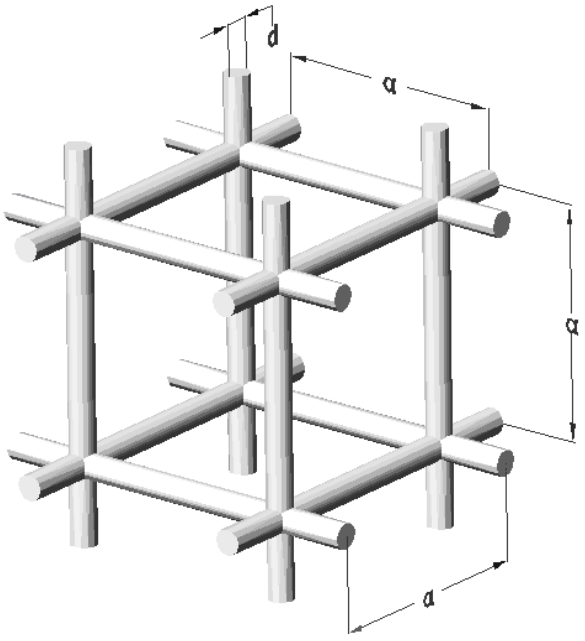

(b)

Figure 7. Open-celled foam under forced convection: (a) notations, (b) cubic unit cell [21].

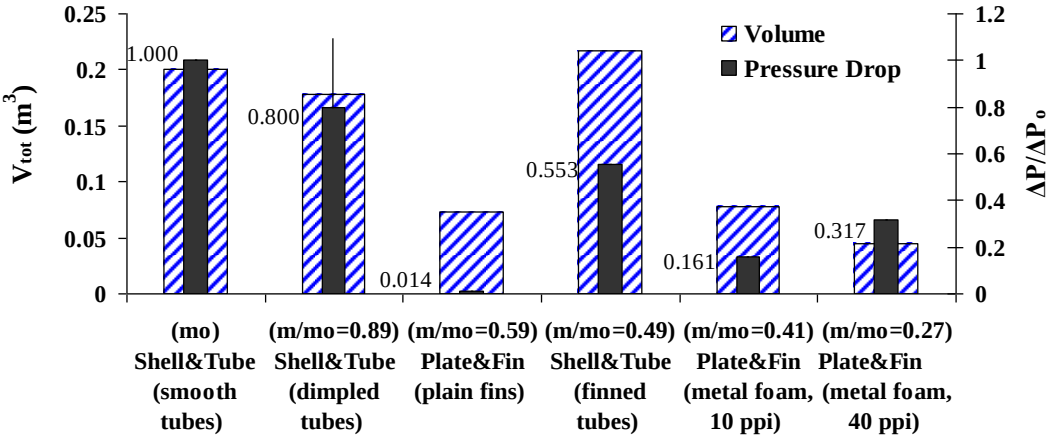

Figure 8. Relative Pressure Drop (right axis and data labels), Volume (left axis) and Relative Mass (x-axis titles) of the heat exchanger configurations that were studied. Dimpled tube pressure drop range is also shown.

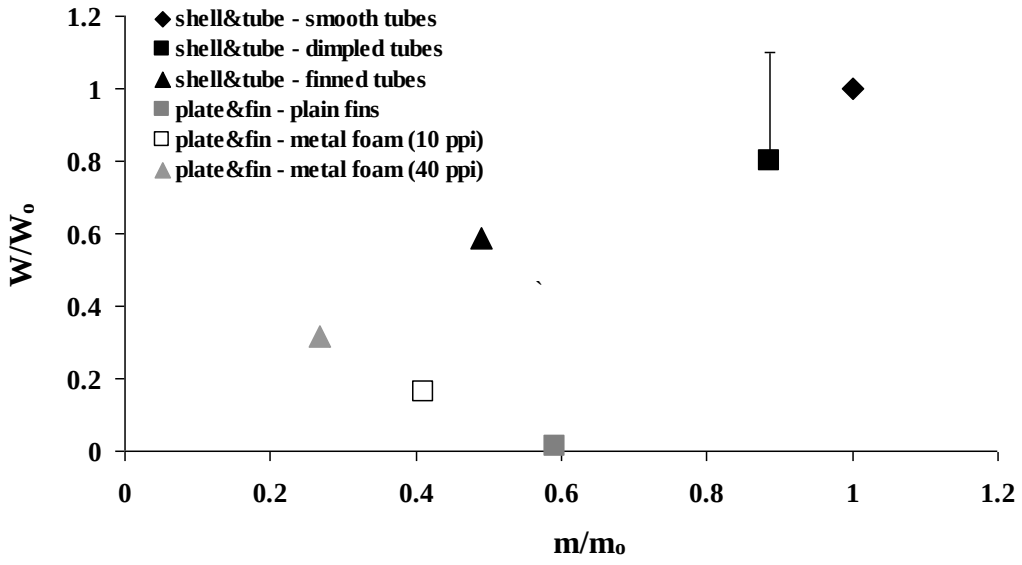

Figure 9. Relative pumping power in terms of relative mass for each of the heat exchanger configurations studied.

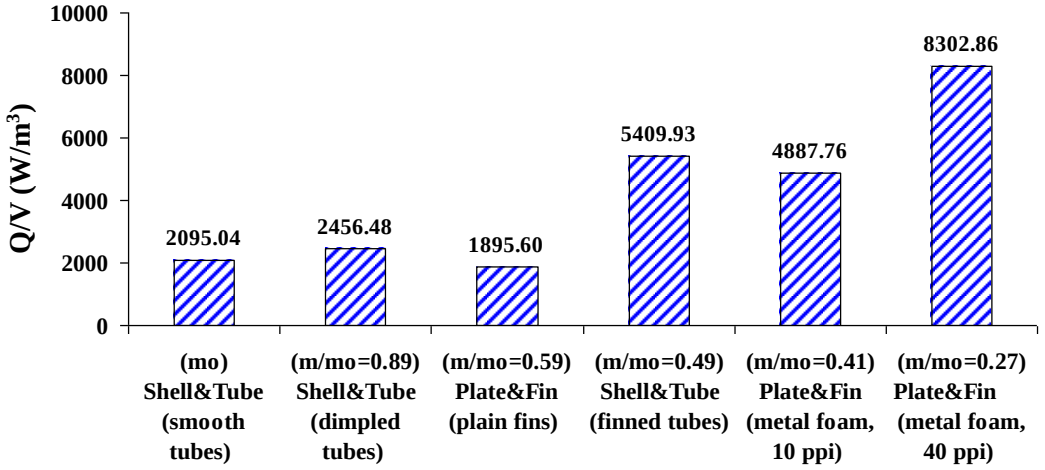

Figure 10. Heating power transferred per unit volume for each of the heat exchanger configurations considered.

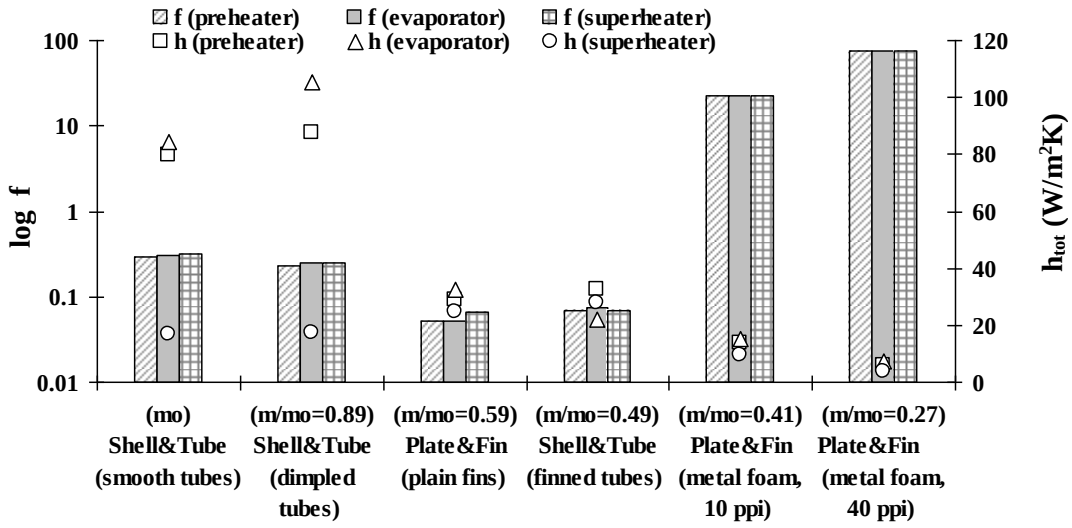

Figure 11. Total heat transfer coefficient (right axis) and friction factor (logarithmic left axis) for each of the heat exchanger configurations studied.

Table 1 Matrix of diesel engine operating conditions examined in the investigation [19].

Load (%)	Speed (rpm)	Exhaust Gas Temperature (ºC)	Heat Transfer at Exchanger (kW)	Exh. Gas Flowrate (kg/s)
100	1300	503.5	136.44	0.490
75	1300	459.3	91.30	0.395
50	1300	394.2	55.45	0.306
25	1300	363.1	33.93	0.205
100	1700	483.7	128.37	0.512
75	1700	423.3	89.26	0.441
50	1700	353.6	60.18	0.368
25	1700	334.5	36.67	0.246
100	2100	435.2	92.27	0.439
75	2100	382.4	71.32	0.410
50	2100	317.6	51.62	0.352
25	2100	291.0	34.19	0.269

Table 2 Typical diesel exhaust gas HEX data used for calculations [19].

		Preheater	Evaporator	Superheater
Heat rate (kW)		31.41	85.27	19.76
Water-steam flow (kg/s)		0.048	0.048	0.048
Exhaust gas flow (kg/s)		0.49	0.49	0.49
Water-steam press. (bar)		33	33	33
Exhaust gas press. (bar)		1	1	1
Exhaust gas temp. (ºC)	$T_{h,1}$	318.02	469.2	503.5
	$T_{h,2}$	261.2	318.02	469.2
Water-steam temp. (ºC)	$T_{c,1}$	90.56	239.2	239.2
	$T_{c,2}$	239.2	239.2	394.2

Table 3 Parameters used for the Shell and Tube HEX calculations.

	Preheater	**Evaporator**	**Superheater**
Baffle cut (%)	20	20	20
Number of baffles, N_b (m)	2	2	2
Int. tube diameter, $d_{t,i}$ (mm)	12	12	12
Ext. tube diameter, $d_{t,o}$ (mm)	16	16	16

Table 4 Increment coefficient of heat transfer, used for dimpled tubes [12].

	η		
	Preheater	**Evaporator**	**Superheater**
Shallow dimples	1.35	1.43	1.35
Deep dimples	1.25	1.4	1.4

Table 5 Fin characteristics for the plate and fin heat exchanger consisting of plain fins [20].

Fin pitch (fins/m)	404
Plate spacing, $P_p = P_{p,h} = P_{p,c}$ (m)	0.01382
Fin metal thickness, $t_f = t_{f,h} = t_{f,c}$ (m)	0.000254
Total heat transfer area/volume between plates, $\beta = \beta_h = \beta_c$ (m^2/m^3)	951.1
Fin area/total area, $A_f/A_{heat} = (A_f/A_{heat})_h = (A_f/A_{heat})_c$	0.863

Table 6a Calculation results for the shell and tube types of heat exchangers.

		Preheater	Evaporator	Superheater
	Q (kW)	**31.41**	**85.27**	**19.76**
Shell&Tube, smooth tubes **Shell dia = 0.49 m** **V_{tot} = 0.2 m^3**	**$d_{t,o}$(mm)**	16	16	16
	N_t	342	342	342
	L (m)	0.215	0.42	0.43
	Tube passes	4	2	2
	P_{row} (m)	0.019	0.019	0.019
	P_{col} (m)	0.022	0.022	0.022
	A_{heat} (m^2)	3.68	7.18	7.38
	h (W/m^2K)	79.48	84.15	16.72
	V (m^3)	0.0405	0.079	0.081
Shell&Tube, finned tubes **Shell dia = 0.49 m** **V_{tot} = 0.217 m^3** **$\Delta p/\Delta p_o$ = 0.553** **$\dot{W}/\dot{W}_o$ = 0.59** **m/m_o = 0.49**	**$d_{t,o}$(mm)**	16	16	16
	N_t	99	110	81
	L (m)	0.24	0.73	0.18
	Tube passes	4	2	2
	P_{row} (m)	0.03428	0.03428	0.03428
	P_{col} (m)	0.03958	0.03958	0.03958
	A_{heat} (m^2)	8.16	27.57	5
	h (W/m^2K)	32.64	21.96	27.7
	V (m^3)	0.045	0.138	0.0339
Shell&Tube, shallow dimpled tubes **Shell dia = 0.49 m** **V_{tot} = 0.176 m^3** **$\Delta p/\Delta p_o$ = 0.8-1.1** **$\dot{W}/\dot{W}_o$ = 0.8-1.1** **m/m_o = 0.88**	**$d_{t,o}$(mm)**	16	16	16
	N_t	342	342	342
	L (m)	0.19	0.33	0.415
	Tube passes	4	2	2
	P_{row} (m)	0.019	0.019	0.019
	P_{col} (m)	0.022	0.022	0.022
	A_{heat} (m^2)	3.25	5.66	7.08
	h (W/m^2K)	90.1	106.7	17.43
	V (m^3)	0.0358	0.0622	0.078
Shell&Tube, deep dimpled tubes **Shell dia = 0.49 m** **V_{tot} = 0.178 m^3** **$\Delta p/\Delta p_o$ = 0.8-1.1** **$\dot{W}/\dot{W}_o$ = 0.8-1.1** **m/m_o = 0.89**	**$d_{t,o}$(mm)**	16	16	16
	N_t	342	342	342
	L (m)	0.195	0.335	0.415
	Tube passes	4	2	2
	P_{row} (m)	0.019	0.019	0.019
	P_{col} (m)	0.022	0.022	0.022
	A_{heat} (m^2)	3.35	5.74	7.09
	h (W/m^2K)	87.42	105.27	17.4
	V (m^3)	0.0368	0.063	0.078

Table 6b Calculation results for the plate and fin types of heat exchangers.

		Preheater	Evaporator	Superheater
	Q (kW)	**31.41**	**85.27**	**19.76**
Plate&Fin, plain fins **V_{tot} = 0.0726 m^3** **$\Delta p/\Delta p_o$ = 0.014** **$\dot{W}/\dot{W}_o$ = 0.0136** **m/m_o = 0.59**	**N_p**	46	46	46
	$A_{heat,tot}$ (m^2)	20.32	37.3	9.98
	A_{plates} (m^2)	1.59	2.93	0.78
	A_{fins} (m^2)	18.73	34.4	9.19
	h (W/m^2K)	28.79	32.45	24.88
	V (m^3)	0.0218	0.04	0.0107
	L (m)	0.63	0.63	0.63
	D (m)	0.055	0.101	0.027
	W (m)	0.63	0.63	0.63
Plate&Fin – metal foam, 10 ppi **V_{tot} = 0.0775 m^3** **$\Delta p/\Delta p_o$ = 0.161** **$\dot{W}/\dot{W}_o$ = 0.16** **m/m_o = 0.41**	**N_p**	27	27	27
	A_{plates} (m^2)	0.937	1.687	0.575
	A_{MF} (m^2)	20.91	37.65	12.83
	h (W/m^2K)	312.19	358.66	214.9
	V (m^3)	0.0227	0.0409	0.0139
	L (m)	0.63	0.63	0.63
	D (m)	0.0572	0.103	0.0351
	W (m)	0.63	0.63	0.63
Plate&Fin – metal foam, 40 ppi **V_{tot} = 0.0448 m^3** **$\Delta p/\Delta p_o$ = 0.317** **$\dot{W}/\dot{W}_o$ = 0.318** **m/m_o = 0.27**	**N_p**	27	27	27
	A_{plates} (m^2)	0.547	0.893	0.41
	A_{MF} (m^2)	48.84	79.69	36.55
	h (W/m^2K)	535.78	680.9	309.22
	V (m^3)	0.0133	0.0216	0.0099
	L (m)	0.63	0.63	0.63
	D (m)	0.0334	0.0545	0.025
	W (m)	0.63	0.63	0.63